Cooling of the West Spitsbergen Current: AUV-based Turbulence Measurements West of Svalbard

E. Steele
Plymouth University
Plymouth, U.K.
Email: edward.steele@plymouth.ac.uk

T. Boyd, M. Inall, E. Dumont and C. Griffiths
Scottish Association for Marine Science (SAMS)
Oban, U.K.

***Abstract*—The role of turbulence is critical in the redistribution of heat and salt throughout the global ocean, and in boundary currents of the high-latitude oceans in particular. In the Arctic Ocean, warm, saline waters of Atlantic origin, which are carried northwards by the West Spitsbergen Current (WSC), are the largest source of oceanic heat carried into the Arctic Eurasian basin, and may have a significant impact on the rate of sea ice decline. While the rapid down-stream cooling of the WSC around its entry point into the Arctic Ocean is well-known, the processes by which this heat flux occurs are still an area of active research. During a cruise to the Svalbard region in July 2010, a Hydroid REMUS 600m AUV, equipped with a forward-mounted microstructure package, was used to quantify the level of turbulent mixing within and across the shoreward edge of the WSC. The microstructure-equipped AUV was used to measure horizontal profiles of water properties and turbulence parameters while a more-conventional, vertically free-falling microstructure profiler was used to conduct complementary transects of vertical profile measurements across the edge of the WSC. In this study we evaluate the resulting measurements and compare the views of the upper ocean derived from similar sensors mounted on two very different platforms: one view assembled from conventional vertical profiles and the second from horizontal, AUV-based profiles. We discuss the impact of mixing on the cooling of the WSC and the capacity of these platforms to resolve small-scale variability in both the vertical and the horizontal.**

I. Introduction

The boundary between the warm, saline waters of Atlantic origin carried northwards by the West Spitsbergen Current (WSC) and the surrounding cool, fresh polar waters is marked by a density compensated ocean front west of Svalbard [1]. The steep bathymetry of the area serves to steer the current along the continental slope to the west of the archipelago (in accordance with conservation of the potential vorticity) that, in turn, moderates the location of these interfaces with respect to shelf / slope position [1], [2]. To the north-west of Svalbard, the WSC splits into two branches at the base of the Yermak Plateau: one flowing north-east (probably suppling most of the Atlantic water entering the Arctic) and another following a north-west path both along the Yermak Plateau and feeding into a recirculating eddy field around Fram Strait [2], [3]. This is accompanied by a rapid down-stream cooling of these Atlantic waters (which represent the largest source of oceanic heat carried into the Arctic Eurasian basin), with heat lost to the atmosphere, sea-ice melt and mixing with the surrounding (on shelf) water [4], [5]. Away from the sea-surface, however, this heat flux is still poorly understood, with the exchanges occurring across fronts thought most significant in promoting mixing beyond depths of 50-100 m [6].

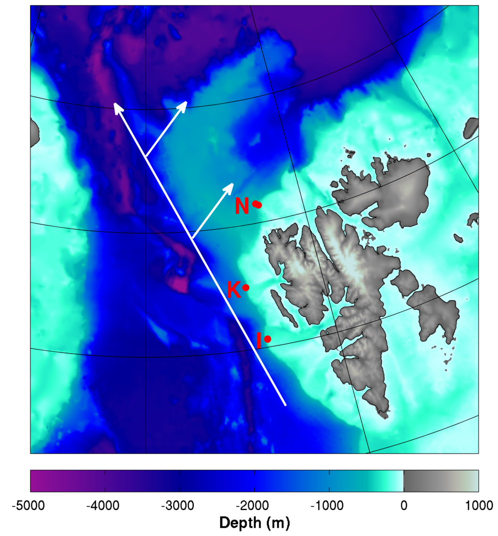

Fig. 1. Location of the three AUV/MSS deployments conducted on Cruise JR219, identified by red markers and labelled (south-north): 'I' (Isfjordbanken), 'K' (Kongsfjordbanken) and 'N' (Norskebanken). The white arrows represent the core of the WSC.

To quantify the level of frontal mixing within and across the shoreward edge of the WSC, measurements of salinity, temperature and the Turbulent Kinetic Energy (TKE) dissipation rate, ϵ, were made at three sites over the western and northern continental margin of Spitsbergen. The measurements were collected with two very different platforms: an autonomous underwater vehicle (AUV), conducting measurements which are at very high horizontal resolution but relatively coarse vertical resolution, and a vertical profiler, conducting measurements which are at very high vertical resolution but relatively coarse horizontal resolution. The locations of these three sampling areas are illustrated in Fig. 1, where the red markers correspond to the two ends of the AUV transects (labelled 'I', 'K', 'N', south-north respectively) and the white arrows represent the path of the core of the WSC along the slope. Although these three sets of data will enable comparison of latitudinal differences along the path of the WSC, we focus here on only the cross-frontal characteristics of the most

TABLE I
AUV AND MSS TURBULENCE DATA PROCESSING PARAMETERS.

Platform-Sensor	f (Hz)	U (m/s)	Spatial Resolution (mm)	Nyquist (cpm)	Integration Limits (cpm)	Sampling Interval (s)	Spectrum Window, Overlaps (s), (%) [a]
AUV-RSI	512	2.00	3.90	128	0.75-150	3.00	1.00, 50
MSS-PNS	416	0.80	1.90	260	2-(K_k-2)	1.25	1.23, 50

[a] K_k = Kolmogorov wavenumber

southerly of the three stations. This section is west of Isfjorden, at the site labelled 'I' on Fig. 1. In addition, we compare the two views of the upper ocean derived from similar sensors mounted on these two very different platforms.

II. METHODS

A. AUV Measurements

The AUV measurements discussed here were made using a Hydroid REMUS 600 m AUV. The REMUS is a positively buoyant, propeller-driven vehicle, 32.4 cm in diameter and 2.74 m in length, which operates at typical speeds of 3-4 knots through the water. The principal AUV-based scientific sampling discussed here consists of horizontal transects constructed from stacked horizontal profiles of TKE dissipation rate, conducted by a forward-mounted Rockland Scientific International turbulence microstructure suite. This package includes two shear probes, two fast-response (FP07) thermistors a pressure sensor and 3D accelerometers (also used in the calculation of the rate of the TKE dissipation). In addition, a free-flow (unpumped) Neil Brown Ocean Sensors conductivity-temperature (CT) sensor is integrated into the nose, and both a WETlabs chlorophyll-a fluorometer and a 660 nm optical backscatter probe are located in the aft section of the AUV. Integral upward- and downward-looking 600 kHz RDI Acoustic Doppler Current Profilers (ADCPs) are capable of resolving water velocities to about 42 m each side of the vehicle, and bottom-tracking at altitudes of less than 100 m above the seabed to yield velocity over the ground. Underwater navigation is by dead-reckoning aided by bottom-tracked velocity between waypoints at which position is updated with surface GPS fixes. Communication to the vehicle at the surface is conducted by WiFi, to typical maximum ranges of 400 m, or Iridium.

B. MSS Measurements

In conjunction with the stacked horizontal profiles collected by the AUV, ship-based transect consisting of a sequence of vertical profiles of TKE dissipation rate were conducted using an ISW Wassermesstecknik free-fall turbulence microstructure shear sensor (MSS90). The instrument is deployed from the stern of the vessel during transects and remains loosely tethered to a shipboard winch, with which it is recovered at the end of each cast. The buoyancy of the profiler is adjusted for the local conditions using modular floats, to obtain a typical fall rate of 0.7-0.9 m/s. In addition, the salinity, temperature and pressure sensors on the MSS provide vertical profiles of water properties as it descends.

C. AUV and MSS Turbulence Data Processing

The critical component of both the MSS and the AUV-based turbulence packages are the airfoil-type shear probes that measure small-scale velocity fluctuations. In each case, a piezoceramic element attached to the axially symmetric airfoil senses the lift-force generated by the transverse components of the flow, generating a voltage output which is proportional to the instantaneous cross-stream velocity field [7]. The two types of shear probe used are, however, subtly different in design: in the case of the AUV probe, the lift forces are transmitted directly to the piezoceramic beam; while in the case of the MSS probe, the airfoil and element are separated by a cantilever to improve mechanical resilience (but may in part affect a slight lessening of its sensitivity). Within each instrument, a pair of shear probes are mounted into the relative flow with their responsive axes orthogonal. The longitudinal axes of the MSS sensors are vertical, responding to forces along the pitch and roll axes, whereas the AUV sensors are mounted horizontally, responding to forces along the vehicle pitch and yaw axes. Subsequent to the measurements discussed here, the AUV sensors on shear channel 1 were found to be slightly corroded, and hence (conservatively) only data from shear channel 2 are presented here. The fundamental measurement of velocity shear squared is integrated over a range of wavenumbers to obtain an overall variance level, which is related to TKE dissipation rate. Details of the processing of horizontal and vertical turbulence measurements are described elsewhere (cf. [8], [7]), however the parameters on which these calculations depend (as well as the resolution achieved by this processing) are provided in summary in Table 1.

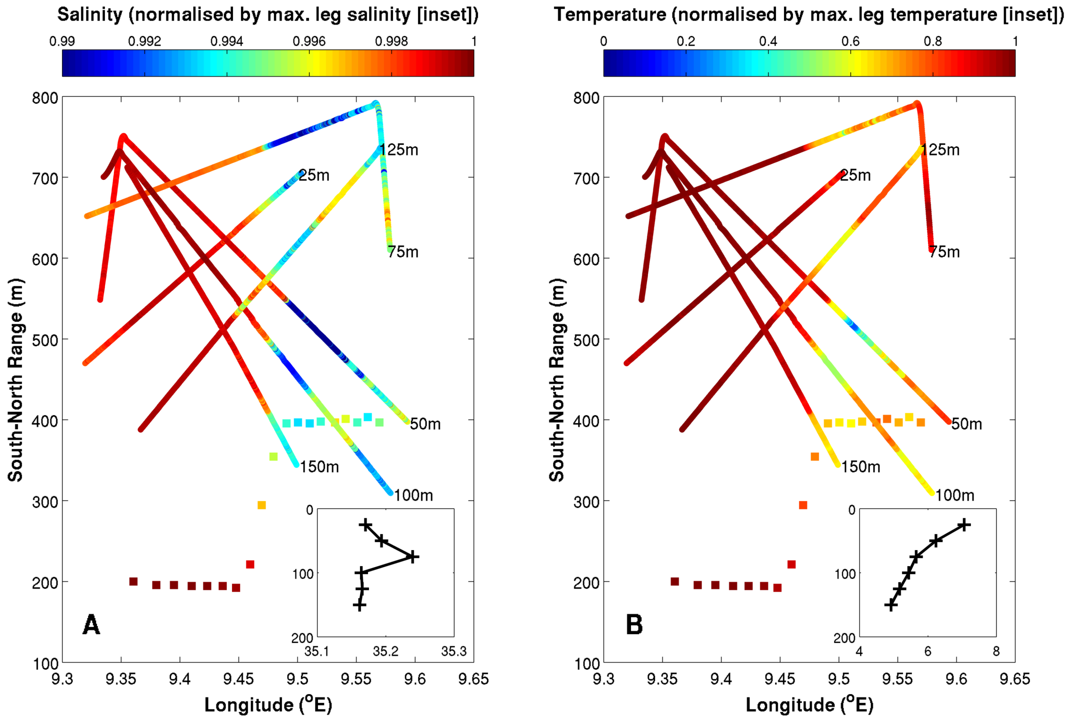

Fig. 2. Location of the WSC front west of Isfjorden as a function of longitude and south-north range, as determined by salinity [A] and temperature [B] transects conducted by the AUV (at depths of 25 m, 50 m, 75 m, 100 m, 125 m and 150 m), normalised by the leg maximum value. The leg maximum value of salinity and temperature (by depth) is included as a profile, inset in both [A] and [B]. MSS temperature and salinity values corresponding to a normalised average of measurements collected between 100 m and 150 m are illustrated by square markers. Attention is drawn to the scale stretching, where 0.05 ^{o} longitude = 1.14 km at 78 ^{o}N.

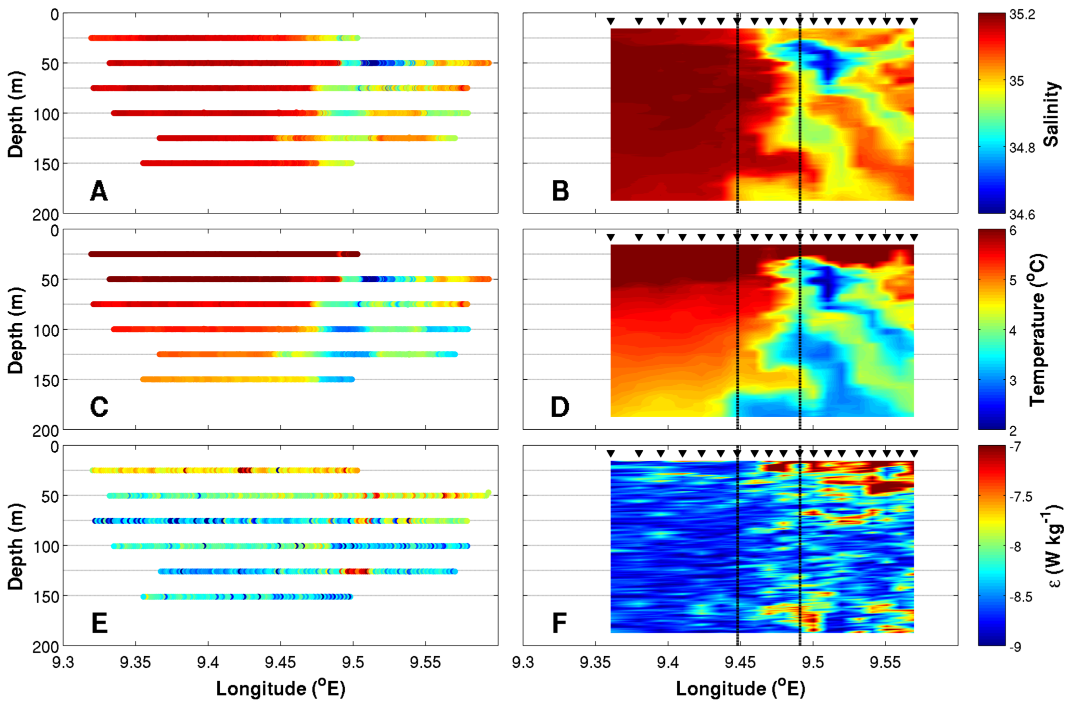

Fig. 3. The vertical structure of the edge of the WSC, where the salinity [A & B], temperature [C & D] and TKE dissipation rate [E & F], as sampled by the AUV and the MSS, respectively, projected onto a line of constant latitude. The area between the vertical black lines in panels [B, D, and F] represents the fold in the ship track between latitudes of 78.1277 ^{o}N (west) and 78.1295 ^{o}N (east).

III. Results

The data used for the present paper were collected with the AUV and MSS deployed simultaneously, west of Isfjorden, on 20 July 2010. For these measurements, the AUV missions were run as a series of legs on alternate headings of 270^o and 90^o over a sequence of depths through the water column. Each of the legs was of nominal length 5 km, and took roughly 45 minutes to complete at 4 knots. Six depths (25 m, 50 m, 75 m, 100 m, 125 m and 150 m) were selected to achieve equal leg-spacings of 25 m in the vertical. The AUV surfaced at the end of each leg to take a GPS fix, with navigation via dead reckoning when submerged. Within ADCP bottom-tracking range, sub-surface navigational accuracy is within typically about 4% of the range travelled underwater [8] – approximately 200 m with 5 km legs between the GPS fixes. Navigation accuracy is significantly worse when the AUV is out of bottom-tracking range, particularly in previously un-sampled areas where the vehicle has not populated a compass bias table, resulting in errors of the order of 10% of the range travelled underwater. Similarly, the reliability of ADCP-derived water velocity estimates is adversely affected by the lack of bottom-tracking. In the present case, four of the six legs were conducted out of bottom-tracking range, and the resulting velocity data consequently do not warrant discussion in this work. The MSS profiling was undertaken as a sequence of 19 profiles to 200 m depth that were collected over 5.26 km track at an average vessel speed of 1 kts (0.5 m/s) , resulting in an average spatial resolution of 292 m, although the ship speed over ground varied by up to 0.7 m/s, with a large changes in heading also occurring.

The distributions of temperature and salinity along both the AUV and ship tracks are shown in Fig. 2, where the characteristic warm (4-6 ^{o}C), salty (35) water of the WSC (to the west of 9.5 ^{o}E) is separated by a rather sharp but variable front from fresher, sometimes cooler water of the continental shelf. The AUV track shows that the vehicle heading was biased south of its intended waypoints on both the westward (25 m, 75 m, and 125 m) legs and the eastward (50 m, 100 m, and 150 m) legs, accumulating errors of up to 400 m over about 5 km (8% of distance travelled). AUV along-track temperatures and salinities shown in Fig. 2 are normalised by the leg-maximum values, with those maximum values shown as vertical profiles (characteristic of the WSC at the western end of the transects) in the figure panels inset. Also shown are the MSS 100-150 m profile averaged values of temperature and salinity In each case, the normalisations allow the front to be visualised.

The vertical structure of the edge of the WSC is seen in Fig. 3, where the salinity, temperature and TKE dissipation rate, as sampled by the AUV (panels 3A, 3C and 3E) and the MSS (panels 3B, 3D and 3F), are shown projected onto a line of constant latitude. Here, the significant west-east differences in the water properties across the front are apparent in both the AUV and MSS signals. The most striking distinction is the difference between the water masses over the shelf and upper water column over the slope, with the slope completely occupied by water of Atlantic origin and the shelf partially occupied by Arctic-modified water with properties typical of the East Spitsbergen Current [1]. Also significant is the increase in variability at smaller vertical and horizontal scales to the east of the frontal region, broadly identified as the region between 9.45 ^{o}E and 9.5 ^{o}E, as indicated by the 'fold' in the ship track in panels 3B, 3D, and 3E. On the western side of the boundary, the salinity and temperature structure compares well to the shape of the leg maximum profiles seen in Fig. 2 (inset): salinity increases from 35.15 to 35.25 between 25 m and 75 m before returning to a value of 35.1 below 100 m, while temperature decreases from 8 ^{o}C at 25 m to 4.5 ^{o}C at 150 m. In contrast, on the eastern side of the boundary, salinity and temperature profiles are more 'patchy' in nature (with values ranging from 34.6 to 35.2 and from 2 ^{o}C to 6 ^{o}C, in turn). A similar pattern is revealed in the TKE dissipation characteristics, with mixing seen to be more energetic in the shorewards half of the front than in the WSC itself.

Qualitative comparisons between the AUV and MSS data suggest very similar salinity and temperature structures are obtained, as well as the same general structure in TKE dissipation rate. This is not only apparent in data from within the WSC to the west, but also within the 'patchy' areas on its eastern side. In particular, three discrete pockets of cool, fresh water (with salinity/temperature values of 34.6/2 ^{o}C, 34.9/3 ^{o}C and 34.9/3.1 ^{o}C) are well resolved by both instruments at 50 m/9.525 ^{o}E, 100-150 m/9.5 ^{o}E and 100-125 m/9.55 ^{o}E, respectively. In close proximity to those pockets are patches of high mixing detected by both sets of turbulence sensors at longitudes of between 9.5 ^{o}E and 9.55 ^{o}E, at depths of 50 m and 75 m with dissipation estimates of the order of $10^{-7.5}$ Wkg^{-1}. Finally, in panel 3E, an additional 'event' is seen at a longitude of 9.5 ^{o}E and a depth of 125 m, coincident with the lowest salinity-temperature extrusion across the front. A similar scale patch at the same longitude is seen in panel 3F at a depth of between 150 m and 180 m. It is possible that this high-TKE patch seen by the AUV and MSS is related to the same eddy feature. AUV and MSS measurements are separated both spatially and temporally (compounded by advection of the water), although it is noted that such high mixing patches at depths $>$ 150 m depth are seen by the MSS to occur in the high salinity lateral boundaries of a low salinity tendril, whereas the high AUV values appear to exist within a low salinity area. Overall, this picture of temperature, salinity, and TKE dissipation rate is consistent with the description [1] of a frontal instability as the main source of subsurface heat loss from the eastern side of the WSC.

Detailed comparisons between salinity and temperature measurements by the two platforms have been conducted using the AUV along-track data from each leg, together with depth-averaged values from the MSS profile data, extracted from 10 m above and below the vehicle depth. A plot of the comparison for temperature is shown in Fig. 4, where error bars represent the standard deviation within the 20 m bins. The similarity in the fields measured by the two sensors is evident. Some

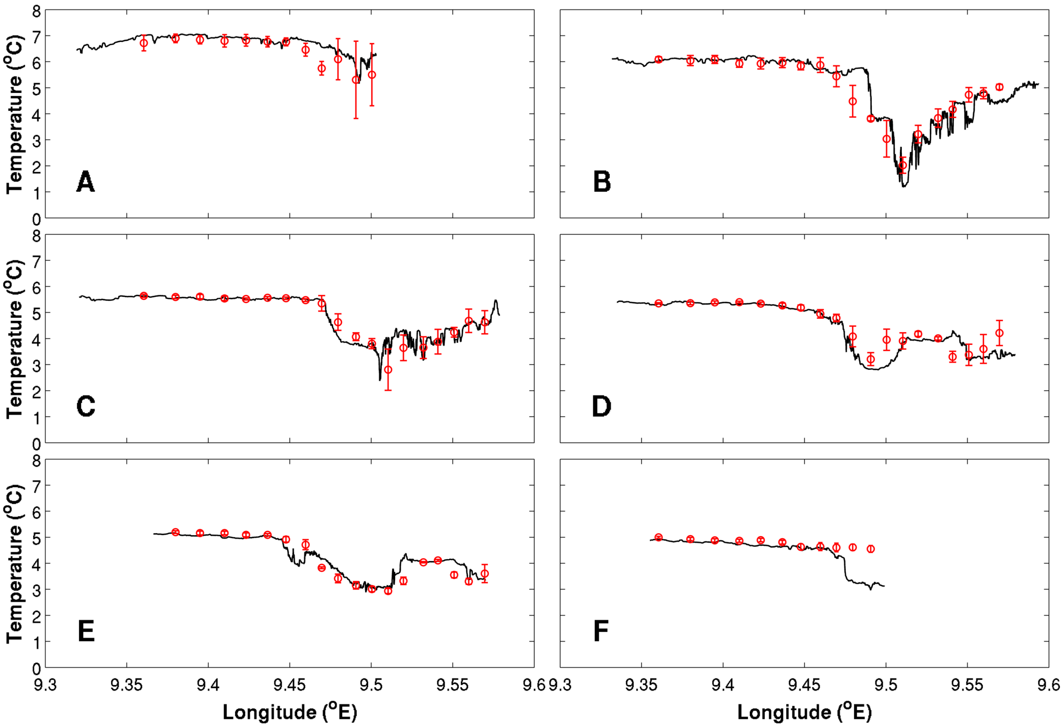

Fig. 4. Detailed comparisons between temperature measurements by the AUV and MSS. The AUV along-track data from each leg is seen, together with depth-averaged values from the MSS profile data (extracted from 10 m above and below the vehicle depth), where the error bars represent the standard deviation within the 20 m bin.

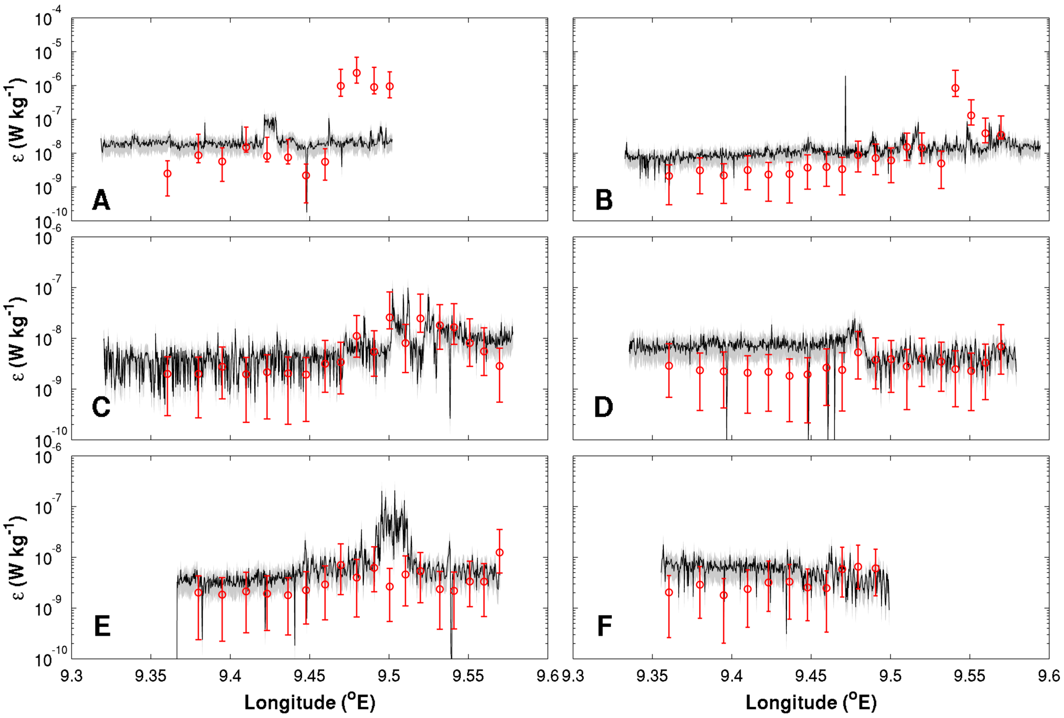

Fig. 5. Detailed comparisons between turbulence measurements by the AUV and MSS. The AUV along-track data from each leg (within an uncertainty envelope of ±50%) is seen together with depth-averaged values from the MSS profile data (extracted from 10 m above and below the vehicle depth), where the error bars represent the 95% bootstrap confidence interval of the mean of the 20 m bin.

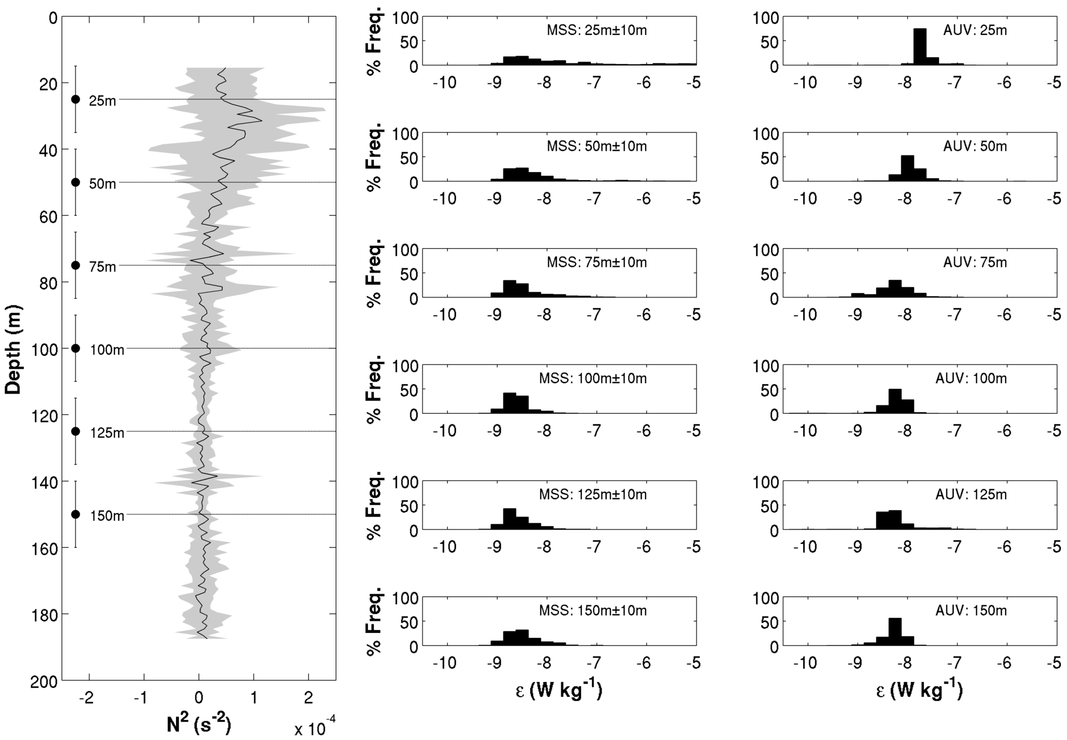

Fig. 6. The probability distributions of TKE dissipation rates, plotted as histograms for the AUV and MSS respectively. Here, the AUV histograms consist of all ϵ values for the leg and the MSS histograms consist of all ϵ values within a bin extending 10 m each side of the target AUV depths of 25 m, 50 m, 75 m, 100 m, 125 m and 150 m. The vertical profile of the square of the buoyancy frequency (computed from the MSS data) is also shown, where the shaded area represents the difference between maximum and minimum of all the profiles.

differences do occur, however, where the AUV and MSS temperature measurements are offset in latitude (e.g. depths of 50 m, panel 4B, and 100 m, panel 4D), which we attribute to the spatial and temporal separations between the sampling conducted by the two platforms (compounded by advection and the dynamics of the front itself). In the case of the 50 m leg, at a latitude of 9.48 ^{o}E, the spatial difference is more than 100 m (although the temporal difference is less than one hour), while the inverse is true in the case of the 100 m leg, at a latitude of 9.54 ^{o}E. The good agreement between salinity and temperature measurements also highlights the benefit of using the two different instruments to guide the interpretation of each other. In panel 4E, a small-scale eddy of less than 500 m in diameter is observed by the AUV at a longitude of 9.45 ^{o}E. Features of this scale are beyond the horizontal resolution of our MSS transect of profiles, but any particular feature of this scale would be unlikely to observe by both platforms, due to along front variability and advection by the mean and variable currents.

A similar comparison between TKE dissipation rate estimates derived from the AUV and MSS is shown in Fig. 5. In this case, the shaded envelope surrounding the along-track AUV values represents the uncertainty from an individual measurement of 50% (assuming a similar estimate to a vertical profiler, [9]), while the depth-averaged MSS values represent the mean values over the window from 10 m above to 10 m below the vehicle, and the error bars represent the 95% bootstrap confidence interval of the mean within the 20 m bins [10]. Although the general depth/longitude structures of the fields measured by both platform/sensor combinations are similar (panels 3E and 3F), details of the longitudinal structure revealed in Fig. 5 are considerably different. This is due in part to the small spatial and temporal scales associated with turbulent patches, as well as some differences in the way in which the two platforms sample the field of turbulent motions. In general, the pattern of the AUV ϵ values suggest a higher TKE dissipation rate than obtained using the MSS, with the exception of estimates on the eastern side of the front at 25 m depth (panel 5A). High MSS ϵ values at 50 m depth to the east of the front (panel 5B) suggest a geophysical, rather than instrumental, source for this elevated signal. This is also consistent with the leg at 75 m depth (panel 5C), where TKE dissipation rates computed with both platform/sensor combinations are higher just east of the front. At depths of 100 m and 150 m (panels 5D and 5F), however, the longitudinal structure of ϵ is different – with a decrease in the amount of mixing reported by the to the east of the front. The evidence for these large-scale dynamics is confirmed in panel 5E, where an eddy (approximately 1.07 km in diameter) is seen at a longitude of 9.5 ^{o}E. The qualitative difference between the distribution of ϵ values at 100 m and 150 m relative to 125 m can be attributed to eddies/frontal instability, and suggest a scale for these of less than 300 m. This figure corresponds to the latitudinal variations in the AUV measurements at 9.45 ^{o}E, that is the separations between the 100 m/150 m AUV crossing of 9.45 ^{o}E from those at 125 m, and also the separation between the MSS measurements at 150 m from the AUV measurements at that depth.

Although differences in detailed structure seen by turbulence sensors mounted on the AUV and MSS platforms is not surprising, especially as there is no shared sample volume (i.e., which is coincident in both space and time), the statistics of the resulting observations are expected to be similar, if they are drawn from the same population of cascading turbulent eddies. The probability distributions of TKE dissipation rates is shown plotted as histograms in Fig. 6 for the data sets from the two platforms, respectively. The MSS histograms consist of all values within bins extending 10 m either side of the target AUV depths of 25 m, 50 m, 75 m, 100 m,125 m, 150 m. The AUV histograms consist of all the ϵ values for the whole leg measured by the AUV. These are shown adjacent to a profile of the square of the buoyancy frequency, to indicate water column stratification. It is often observed that the distribution of TKE dissipation estimates should follow a log-normal distribution [11]. Here, a more Gaussian-type form is observed with both the AUV and the MSS. It is also noted that AUV measurements suggest more a energetic mixing climate than their MSS counterparts, observations thought to be related to vehicle noise (cf. [8]) or the sensor response to vehicle motion (on which work is ongoing).

IV. Conclusion

The Arctic front west of Isfjorden between warm, saline Atlantic waters of the WSC to the west and the cool, fresh polar waters to the east was found to be located at a longitude of approximately 9.5 ^{o}E. Across the shoreward edge of the WSC, a pronounced west-east difference in water characteristics was observed: higher (and more uniform) salinity and temperature structure is apparent on the western side, while the eastern side is exhibits an increased level of Turbulent Kinetic Energy dissipation and patchiness. The results demonstrate that similar vertical structure is captured by both the horizontal sampling of the REMUS AUV and the vertical sampling of the free-falling MSS profile, with good agreement between salinity and temperature sensors mounted on the two instruments (despite the spatial and temporal separation in sampling). Comparison of the turbulence sensors is less consistent due to the small scales of the turbulent fluctuations, however similarity between the probability distributions derived from the two platforms are consistent with samples having been drawn from the same population. Relatively high values of TKE dissipation at water mass boundaries on the inshore side of the front suggest that lateral mixing dominates the transfer of heat from the WSC in summer at this latitude. The successful comparison between dropped profiler and AUV-based measurements of mixing and the resolution of small-scale ($<$ 200 m) structures in the horizontal by the AUV suggest that the AUV is not only a robust platform for these measurements, but also a means to resolve variability close to the sea-surface boundary and within small scale dynamical flow features in climatically critical regions such as the WSC.

Acknowledgment

We thank the Master and crew of the RSS James Clark Ross and the scientists and technical support staff of Cruise JR219. This work was funded by the UK Natural Environment Research Council (under the Oceans 2025 programme), with E.S. funded under a Neil McDougall Bursary, awarded by the Scottish Association for Marine Science (SAMS). We are also grateful to Matthew Toberman for helpful discussions on the sensor characteristics of the SAMS AUV.

References

[1] T. M. Saloranta and H. Svendson, "Across the Arctic front west of Spitsbergen: high-resolution CTD sections from 1998-2000", Polar Res., 20, 177-1184, 2001.

[2] T. M. Saloranta and P. M. Haugan, "Interannual variability in the hydrography of Atlantic water northwest of Svalbard", J. Geophys. Res., 106(C7), 13931-13944, 2001.

[3] R. G. Perkin and E. L. Lewis, "Mixing in the West Spitsbergen Current", J. Phys. Oceanogr., 14, 1315-1325, 1984.

[4] K. Aagaard, A. Foldvik and S. R. Hillman, "The West Spitsbergen Current: disposition and water mass transformation", J. Geophys. Res., 92(C4), 3778-3784, 1987.

[5] T. J. Boyd and E. A. D'Asaro, "Cooling of the West Spitsbergen Current: wintertime observations west of Svalbard", J. Geophys. Res., 99(C11), 22597-22618, 1994.

[6] T. M. Saloranta and P. M. Haugan, "Northward cooling and freshening of the warm core of the West Spitsbergen Current", Polar Res. 23, 79-88, 2004.

[7] H. Prandke, "Microstructure sensors", in Marine Turbulence: Theories, Observations and Models, H. Baumert, J. Simpson and J. Sundermann, Eds. Cambridge: Cambridge University Press, 2004.

[8] T. Boyd, M. Inall, E. Dumont and C. Griffiths, "AUV observations of mixing in the tidal outflow from a Scottish sea loch", IEEE/OES Autonomous Underwater Vehicles (AUV), September 2010.

[9] J. H. Simpson, W. Crawford, T. P. Rippeth, A. R. Campbell and J. V. S. Chaok, "The vertical structure of turbulent dissipation in shelf seas", J. Phys. Oceanogr., 26, 1579-1590, 1996.

[10] T. P. Rippeth and M. E. Inall, "Observations of the internal tide and associated mixing across the Malin shelf", J. Geophys. Res., 107(C4), 3028, 2002.

[11] H. W. Wijesekera, T. M. Dillon and L. Padman, "Some statistical and dynamical properties of turbulence in the oceanic pycnocline", J. Geophys. Res., 98(C12), 22665-22679, 1993.